

HyPCA-Net: Advancing Multimodal Fusion in Medical Image Analysis

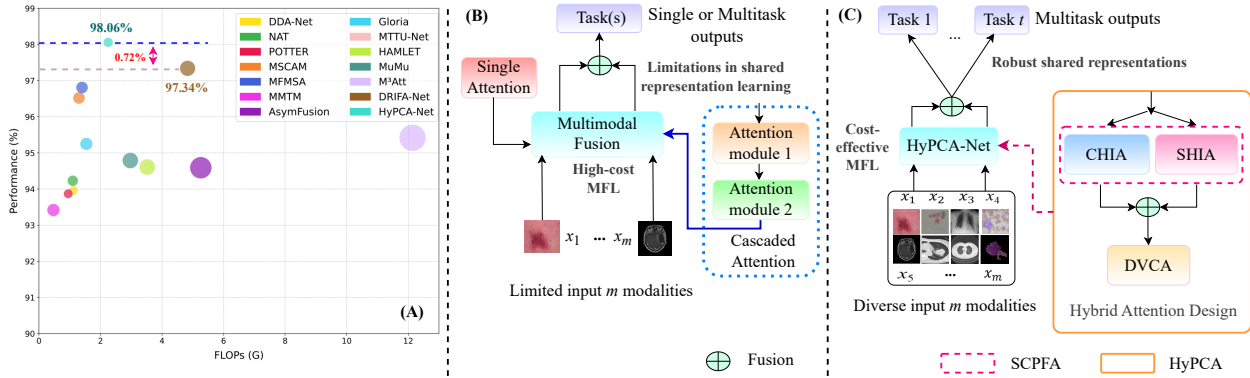
Joy Dhar^{1,*}Manish Kumar Pandey^{2,*}Debashis Das Chakladar^{3,*}Maryam Haghigat⁴Azadeh Alavi⁵Sajib Mistry⁶Nayyar Zaidi⁷¹Indian Institute of Technology Ropar, India²RoentGen Health, India³Lulea University of Technology, Sweden⁴QUT, Australia⁵RMIT University, Australia⁶Curtin University, Australia⁷Deakin University, Australia

Figure 1. (A) Performance comparison between unimodal baselines (e.g., DDA-Net [7], NAT [12], POTTER [39], etc.) and computationally expensive multimodal fusion learning (MFL) methods (e.g., DRIFA-Net [10], HAMLET [16], and MuMu [17], etc.) versus our proposed framework – HyPCA-Net. Bubble size reflects parameter count (larger bubbles = more parameters). (B-C) High-level comparison of three attention mechanisms, namely single attention [12, 39]; cascaded attention [10]; and our proposed hybrid attention (HyPCA-Net). (C) An overview of HyPCA-Net, featuring a HyPCA block that integrates (i) parallel spatial–channel fusion via CHIA and SHIA within the SCPFA module, and (ii) cascaded hybrid-space dual-domain modeling via the DVCA module.

Abstract

Multimodal fusion frameworks, which integrate diverse medical imaging modalities (e.g., MRI, CT), have shown great potential in applications such as skin cancer detection, dementia diagnosis, and brain tumor prediction. However, existing multimodal fusion methods face significant challenges. First, they often rely on computationally expensive models, limiting their applicability in low-resource environments. Second, they often employ cascaded attention modules, which potentially increase risk of information loss during inter-module transitions and hinder their capacity to effectively capture robust shared representations across modalities. This restricts their generalization in multi-disease analysis tasks. To address these limitations, we propose a Hybrid Parallel-Fusion Cascaded Attention Network (HyPCA-Net), composed of two core novel blocks: (a) a computationally efficient residual adap-

tive learning attention block for capturing refined modality-specific representations, and (b) a dual-view cascaded attention block aimed at learning robust shared representations across diverse modalities. Extensive experiments on ten publicly available datasets exhibit that HyPCA-Net significantly outperforms existing leading methods, with improvements of up to 5.2% in performance and reductions of up to 73.1% in computational cost. *Code:* <https://github.com/misti1203/HyPCA-Net>.

1. Introduction

Multimodal data is vital in real-world applications, especially in medical image analysis. Imaging modalities like MRI, CT, and CXR offer complementary anatomical and functional information crucial for diagnosing tumors and other pathologies [10]. While deep learning has enabled efficient diagnosis, single-modality models even with feature fusion or attention, often under-perform due to noisy inputs and overfitting issues [7, 9, 10, 12, 39]. Multimodal

*These authors contributed equally.

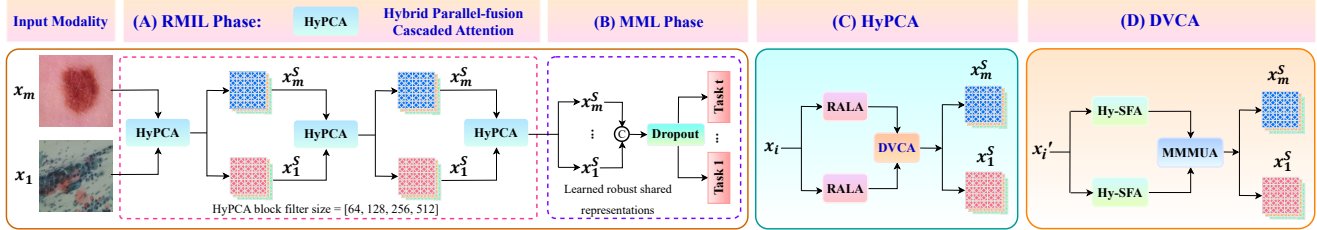


Figure 2. Overview of HyPCA-Net framework composing of two phases: (A) RMIL, which learns robust shared representations $\{x_i^S\}_{i=1}^m$; and (B) MML, which performs multi-disease classification. Within RMIL phase stands our novel (C) HyPCA block comprises of RALA block (refining unimodal features $\{x_i'\}_{i=1}^m$) and (D) DVCA block (capturing dual-domain multimodal information)

fusion mitigates these issues by learning shared representations across heterogeneous modalities [3, 8] (Figure 1 (B)). Attention mechanisms further complement learning by enabling models to focus on salient regions or biomarkers, hence improving representation learning in various medical imaging tasks [15–17, 21] (Figure 1 (B)). Despite recent advances, existing multimodal fusion frameworks [10, 16, 17, 21] incur high computational cost (**challenge 1**) from standard convolutions and multi-stage attention, limiting scalability in healthcare AI. Their sequential (cascaded) attention designs also induce progressive information loss (**challenge 2**) across inter-module transitions, restricting the retention of discriminative patterns and leading to suboptimal performance [23, 35]. These methods do not leverage parallel fusion attention, which can preserve crucial information and enhance representation learning [23, 35].

To address these limitations, we propose a **Hybrid Parallel-fusion Cascaded Attention Network** – HyPCA-Net – a multimodal fusion framework that balances optimal performance with minimal computational cost, while preserving information through both parallel and cascaded attention (Figure 1 (C)). Our proposed framework addresses the aforementioned challenges through two novel blocks: *a Residual Adaptive Learning Attention* (RALA) block and *a Dual-View Cascaded Attention* (DVCA) module, leading to superior performance compared to state-of-the-art methods (Figure 1 (A)). Note that RALA and DVCA together constitute our novel HyPCA block, as shown in Figure 2. Once integrated into a multimodal learning framework comprising two phases—RMIL and MML—we refer to it as HyPCA-Net. Various components of HyPCA-Net, along with the inputs and outputs of each block, are illustrated in Figure 2.

HyPCA-Net balances optimal performance with minimal computational cost across diverse medical imaging modalities. Specifically, the RALA block addresses **both challenges** by learning *enhanced multi-scale spatial–channel representations in parallel* via an efficient Spatial–Channel convolution Adaptive Learning Attention (SCALA) module. This design preserves computational efficiency, enriches representational diversity, and bypasses the sequential bottlenecks of cascaded attention. On the

other hand, DVCA block **tackles challenge 1** by leveraging *cascaded hybrid spaces and dual-domain information integration*. By optimizing multimodal features across these spaces and domains, DVCA learns robust shared representations while reducing computational overhead. By integrating these components, HyPCA-Net is tailored to learn from diverse medical imaging scenarios and exhibits strong generalizability for multi-disease classification. **Our main contributions can be summarized as follows:**

- We propose HyPCA-Net, a multimodal fusion framework that seamlessly integrates parallel fusion attention and cascaded attention modules to learn robust shared representations while achieving optimal performance at minimal computational cost.
- We propose a novel RALA block, which enhances unimodal representations by incorporating multi-scale convolutions with a parallel spatial–channel fusion attention module, thereby progressively refining features through the joint capture of diverse spatial and channel dependencies.
- We introduce a novel DVCA block, a cascaded attention module that integrates dual-domain information within a hybrid representation space to learn robust shared features.
- We conduct extensive experiments on ten diverse medical imaging datasets to demonstrate that HyPCA-Net consistently outperforms state-of-the-art methods.

We summarize all abbreviations used throughout the paper in Table 1 to improve the clarity.

2. Related Works

Earlier multimodal fusion research has extensively focused on natural vision and medical imaging applications [5, 18, 27]. Specifically, existing frameworks e.g., MTTU-Net integrated CNNs and transformers for glioma segmentation and IDH prediction but lacked explicit attention for refined representations [5]. Recent attention-driven designs – DDA-Net [7], MADGNet [25], NAT [12], POTTER [39], and EMCAD – show substantial gains in representation learning [14–17, 21]. Incorporating attention mechanisms into multimodal fusion frameworks – through structural designs such as parallel and cascaded attention modules – has sig-

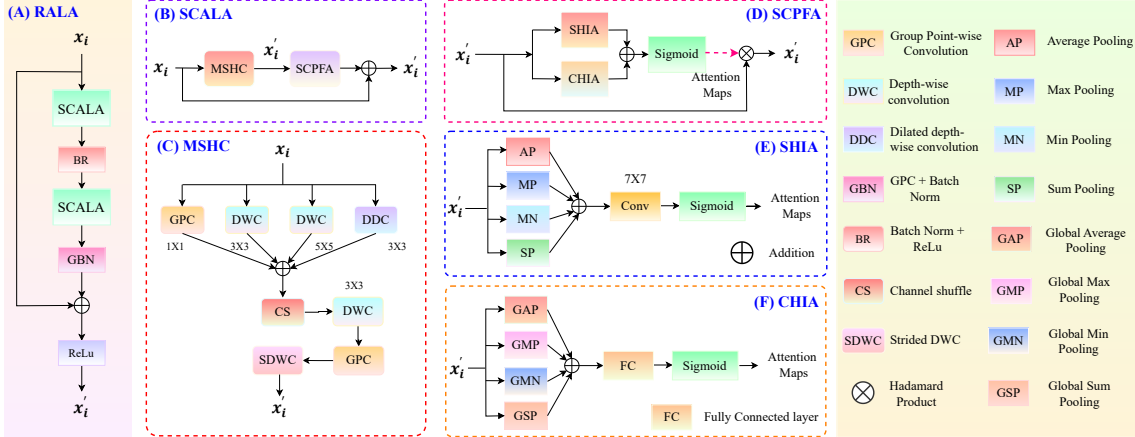


Figure 3. (A) Overview of RALA block (first main component of HyPCA), which is composed of SCALA blocks (B), which in turn is made out of MSHC block (C) and SCPFA block (D). The SCPFA block is composed of SHIA (E) and CHIA (F) components.

Table 1. List of abbreviations based on modules and components.

Abbreviation	Full Term	Appears in
HyPCA-Net	Hybrid Parallel-fusion Cascaded Attention Network	Sec. 1, 3
HyPCA	HyPCA block (RALA + DVCA)	Sec. 3
RMIL	Robust Multimodal Information Learning	Sec. 3.1
RALA	Residual Adaptive Learning Attention	Sec. 3.1.1
SCALA	Spatial-Channel convolution Adaptive Learning Attention	Sec. 3.1.1
MSHC	Multi-scale Spatial Heterogeneous Convolution	Sec. 3.1.1
SCPFA	Spatial-Channel Parallel Fusion Attention	Sec. 3.1.1
SHIA	Spatial Holistic Information-Learning Attention	Sec. 3.1.1
CHIA	Channel Holistic Information-Learning Attention	Sec. 3.1.1
DVCA	Dual-View Cascaded Attention	Sec. 3.1.2
Hy-SFA	Hybrid Space Fusion Attention	Sec. 3.1.2
TSFI	Token-space Frequency-Spatial Integration	Sec. 3.1.2
FDCA	Feature-space Dual-Solver Channel Attention	Sec. 3.1.2
HCA	Heterogeneous Channel Attention	Sec. 3.1.2
MMMUA	Multi-scale Multi-frequency Mutual Update Attention	Sec. 3.1.2
FCIF	Frequency-domain Channel Information Fusion	Sec. 3.1.2
SMIF	Spatial-domain Multi-scale Information Fusion	Sec. 3.1.2
MCBI	Mutual Cross Bidirectional Interactions	Sec. 3.1.2
HCF	Hierarchical Channel Fusion	Sec. 3.1.2
MML	Multimodal Multitask Learning	Sec. 3

nificantly enhanced performance [14–17, 21]. For example, Gloria integrated global-local attention to align radiology images with textual reports for efficient label learning [15], while M³Att employed mutual attention and iterative interaction to fuse visual and language features for referring image segmentation [21]. HAMLET and MuMu utilized hierarchical and guided multimodal attentions for human activity recognition [16, 17]. Methods such as CAF and DRIFANet used co-attention fusion and cascaded dual-attention strategies for skin cancer diagnosis and multi-disease classification [10, 14], showing attention’s versatility. Despite recent progress, prior frameworks remain computationally intensive and prone to information loss across modules, limiting robust representation learning. To overcome this, we propose a hybrid attention-based fusion architecture to balance performance and efficiency, key to scalable healthcare AI. See *supplementary* for more details.

3. Methods

Problem Formulation. Given inputs $X = \{x_i\}_{i=1}^m$ drawn from m heterogeneous modalities and labels $Y = \{y_j\}_{j=1}^t$

for t tasks, our network $\mathcal{F}(\cdot)$ aims to learn robust shared representations $X^S = \{x_i^s\}_{i=1}^m$. This facilitates the mapping $\mathcal{F}(X) \rightarrow Y$, thereby jointly optimizing for high performance with minimal computational cost.

Method Overview. We present a holistic overview of HyPCA-Net framework (ref. Figure 2). HyPCA-Net comprises of two salient phases: **1) Robust Multimodal Information Learning (RMIL)** – Learn robust shared representations. **2) Multimodal Multitask Learning (MML)** – inspired from DRIFANet [10] – it facilitates multiple downstream tasks (e.g., multi-disease classification) and comes after RMIL phase. That is, the resulting shared representations X^S from the RMIL phase is used to classify multiple diseases across $i \in [1 : m]$ modalities. It maps input X to output predictions \mathcal{Y} using a loss function \mathcal{L}_{MML} , where λ_t^i controls the weight of each task-modality-specific loss \mathcal{L}_t^i . The best model parameters β^* are found by minimizing \mathcal{L}_{MML} , i.e.,

$$\mathcal{L}_{\text{MML}} = \sum_{t=1}^T \sum_{i=1}^m \lambda_t^i \cdot \mathcal{L}_t^i(\mathcal{F}(X^S; \beta), \mathcal{Y}); \quad \beta^* = \arg \min_{\beta} (\mathcal{L}_{\text{MML}}), \quad (1)$$

where β signifies the HyPCA-Net parameters. In the following, we will discuss RMIL phase in detail.

3.1. Robust Multimodal Information Learning

The Robust Multimodal Information Learning (RMIL) phase is comprised of m parallel modality-specific branches each containing b cascaded HyPCA blocks (see Figure 2). Each block integrates two attention sub-blocks into a hybrid design by incorporating parallel fusion attention (via **Residual Adaptive Learning Attention (RALA)**) block which captures multi-scale spatial and channel dependencies to learn refined unimodal representations $X' = \{x'_i\}_{i=1}^m$ with cascaded attention (via **Dual-View Cascaded Attention (DVCA)**) block which integrates spatial and frequency domain information to capture robust shared representations

$X^s = \{x_i^s\}_{i=1}^m$). Let us delve into the details of these blocks in the following.

3.1.1. Residual Adaptive Learning Attention

Residual Adaptive Learning Attention (RALA) sub-block (ref. Figure 3(A)) refines representations by jointly capturing multi-scale spatial patterns and channel dependencies with minimal computational cost. It is motivated to address EMCAD [31] shortcomings, i.e., (1) single-stage multi-scale processing, (2) homogeneous branch design, and (3) lack of spatial–channel fusion. RALA addresses these limitations by leveraging a component named Spatial–Channel convolution Adaptive Learning Attention (SCALA) (Figure 3(B)) – which comprises of two core components: A) Multi-scale Spatial Heterogeneous Convolution (MSHC) and B) Spatial–Channel Parallel Fusion Attention (SCPFA). Specifically to achieve cascaded information refinement: RALA replaces the MSDC block of EMCAD with a pair of SCALA modules (ref. Figure 3(A)) enabling progressive multi-scale representations refinement. Secondly, to achieve heterogeneous branch design, each MSHC module employs heterogeneous convolutions at varied scales across branches to promote representational diversity. Finally, to achieve spatial–channel fusion, an SCPFA block jointly learns spatial and channel dependencies resulting enriched representations for downstream tasks. Formally, given a modality-specific input x_i – to obtain refine representations $\{x_i'\}_{i=1}^m$ – RALA(\cdot) block can be written as:

$$\begin{aligned} \text{RALA}(x_i) &= \mathcal{R}\left(x_i + \underbrace{\text{BNPC}(\text{SCALA}(\mathcal{R}(\text{BN}(\text{SCALA}(x_i)))))}_{\text{Progressive Cascaded Refinement}}\right), \\ \text{SCALA}(x_i) &= x_i + \text{SCPFA}(\text{MSHC}(x_i)). \end{aligned} \quad (2)$$

where skip connections stabilize gradient flow and promote feature reuse; $\text{BNPC}(\cdot) = \text{BN}(\text{PC}(\cdot))$ applies batch normalization with point-wise convolution respectively; and $\mathcal{R}(\cdot)$ denotes the ReLU activation. In the following, let us discuss MSHC and SCPFA blocks.

(A) Multi-scale Spatial Heterogeneous Convolution. Multi-scale Spatial Heterogeneous Convolution (MSHC) block (ref. Figure 3(C)) employs heterogeneous convolutional branches obtained with group point-wise convolution (GPC), dilated depth-wise convolution (DDC) and depth-wise convolution (DWC) – with varying scales k (1×1 , 3×3 , 5×5)¹. To further facilitate inter-channel communication, we apply a channel shuffle operation $\text{CS}(\cdot)$. Finally, a sequence of GPC, DWC, and a strided DWC (denoted as SDWC) layers restores the original channel dimensionality, explicitly capturing inter-channel dependencies, and further refining the representation. We summarize operations of $\text{MSHC}(\cdot)$ block as:

¹This design fosters branch-wise heterogeneity, enabling the block to capture fine-grained multi-scale spatial patterns by fusing the outputs from these branches to capture enriched representations $x_i' = \text{MSHC}(\cdot)$, thus enhancing representational diversity.

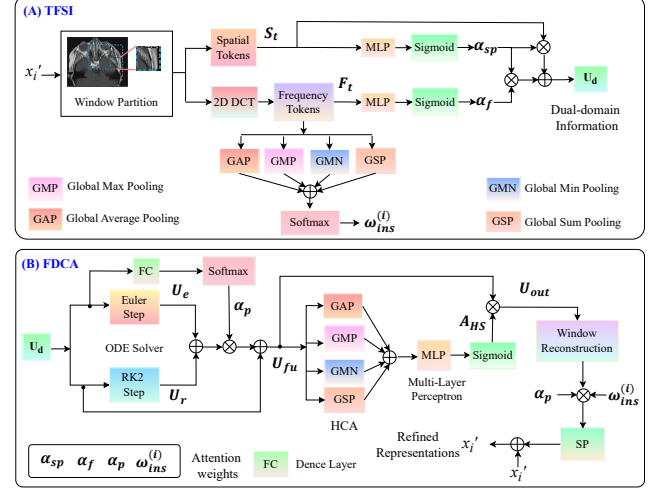


Figure 4. Overview of Hy-SFA (key component of DVCA block) comprising (A) TFSI and (B) FDCA blocks. FDCA includes Heterogeneous Channel Attention (HCA).

$$\text{MSHC}(x_i) = \text{SDWC}\left(\text{GPC}\left(\text{DWC}\left(\text{CS}\left(\theta\left(\bigcup_{k \in \{1,3,5\}} \text{HC}_k(x_i)\right)\right)\right)\right)\right). \quad (3)$$

where $\text{HC} \in \{\text{GPC}, \text{DWC}, \text{DDC}\}$ and θ represents fusion.

(B) Spatial–Channel Parallel Fusion Attention. Spatial–Channel Parallel Fusion Attention (SCPFA) block (ref. Figure 3(D)) enriches modality-specific representations by jointly learning spatial and channel cues. It comprises of two key components: (1) *Channel Holistic Information-Learning Attention* (CHIA) and (2) *Spatial Holistic Information-Learning Attention* (SHIA). To design CHIA (Figure 3(F)) , we apply diverse global pooling operations – global average pooling (GAP), global max pooling (GMP), global min pooling (GMN), and global sum pooling (GSP) – to capture long-range channel contexts. To design SHIA (Figure 3(E)) , we employ multi-perspective local pooling operations – average pooling (AP), max pooling (MP), min pooling (MN), and sum pooling (SP) – to learn fine-grained spatial details. Within each branch, the resulting distinct contexts are fused to capture diverse dependencies, i.e., they apply sigmoid $\sigma(\cdot)$ function to obtain the channel attention map $A_C = \text{CHIA}(\cdot)$ and the spatial attention map $A_S = \text{SHIA}(\cdot)$. We integrate these maps into a joint attention map $A_{SC} = \text{SCPFA}(\cdot)$, which recalibrate the input features x_i' , yielding the refined representations. We write SCPFA(\cdot) block operations as:

$$\begin{aligned} x_i' &= x_i' \odot \text{SCPFA}(x_i'), \\ \text{SCPFA}(x_i') &= \sigma(\text{SHIA}(x_i') + \text{CHIA}(x_i')). \end{aligned} \quad (4)$$

where:

$$\text{CHIA}(x_i') = \sigma\left(\text{FC}\left(\text{GAP}(x_i') + \text{GMP}(x_i') + \text{GMN}(x_i') + \text{GSP}(x_i')\right)\right). \quad (5)$$

$$\text{SHIA}(x_i') = \sigma\left(\text{Conv}\left(\text{AP}(x_i') + \text{MP}(x_i') + \text{MN}(x_i') + \text{SP}(x_i')\right)\right). \quad (6)$$

Here \odot denotes Hadamard product, FC and Conv are dense and convolution layers, respectively.

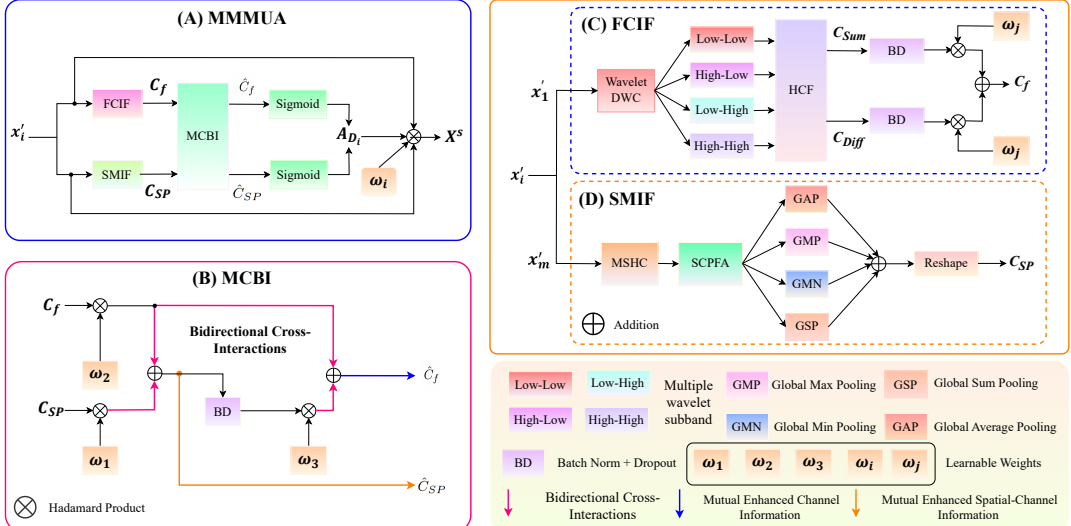


Figure 5. (A) Overview of the MMMUA block (key component of DVCA block). It consists of MCBI (B), FCIF (C), and SMIF (D) blocks. The MCBI block integrates the outputs of FCIF and SMIF blocks. FCIF employs Hierarchical Channel Fusion (HCF) mechanism.

3.1.2. Dual-View Cascaded Attention

Dual-View Cascaded Attention (DVCA) block (Figure 2(D)) aims to learn robust shared representations X^s from multimodal input X' via two cascaded modules, i.e., Hybrid Space Fusion Attention (Hy-SFA) – for capturing modality-specific diverse channel dependencies in hybrid (token and feature) spaces and Multi-scale Multi-frequency Mutual Update Attention (MMFU) – for enriching multi-modal contextual representations by capturing dual domain (spatial and frequency) information. Let us discuss these two blocks in the following.

(A) Hybrid Space Fusion Attention. Token-space attention (e.g., window-based local attention) [22] captures fine-grained spatial interactions, while feature-space method (e.g., frequency-domain attention via 2D DCT) [29] strengthens texture discrimination. Yet these paradigms have not been co-attended within a single module, leaving a gap in hybrid-space interaction for multimodal fusion pipelines. To bridge this gap, we propose the Hybrid Space Fusion Attention (Hy-SFA) module (Figure 4), which enriches each modality input x'_i by jointly capturing diverse channel dependencies across token and feature spaces through two cascaded submodules—TFSI and FDCA—that enable cross-domain context exchange.

- *Token-space Frequency–Spatial Integration* (TFSI) learns complementary dual-domain information by jointly processing spatial and frequency tokens within each local window (Figure 4(A)). Specifically, given an input x'_i and a window size w , we first cyclically shift x'_i by $\lfloor w/4 \rfloor$ pixels along spatial axes and partition it into non-overlapping $w \times w$ windows. In each window, TFSI captures spatial tokens $\mathbf{S}_t \in \mathbb{R}^{w^2 \times C}$ directly from the windowed features and frequency tokens $\mathbf{F}_t \in \mathbb{R}^{w^2 \times C}$

via a normalized 2D discrete cosine transform (DCT). Each token set is processed independently via an MLP (f_θ) followed by a sigmoid σ , yielding attention weights:

$$\alpha_{sp} = \sigma(f_\theta(\mathbf{S}_t)) \quad \text{and} \quad \alpha_f = \sigma(f_\theta(\mathbf{F}_t)). \quad (7)$$

We fuse the weighted token streams by emphasizing informative features from each domain to obtain the dual-domain output \mathbf{U}_d :

$$\mathbf{U}_d = (\alpha_{sp} \odot \alpha_f) + (1 - \alpha_{sp}) \odot \mathbf{S}_t. \quad (8)$$

- *Feature-space Dual-Solver Channel Attention* (FDCA) (Figure 4 (B)) refines dual-domain tokens $\mathbf{U}_d \in \mathbb{R}^{HW \times C}$ in feature space by treating them as the initial state (\mathbf{H}_0) of a continuous-depth flow, following the neural-ODE formulation [4]. A GAP followed by a sigmoid-activated Dense layer applied to \mathbf{H}_0 , yielding the adaptive step size $\tau \in (0, 1]$ for further processing. To capture information at complementary scales, FDCA applies two discrete Ordinary Differential Equation (ODE) solvers in parallel – a first-order Euler step for coarse-grained contexts (\mathbf{U}_e) and a second-order Runge–Kutta (RK2) step for fine-grained details (\mathbf{U}_r) as:

$$\begin{aligned} \mathbf{U}_e &= \mathbf{H}_0 + \tau f_\theta(\mathbf{H}_0), \\ k_1 &= f_\theta(\mathbf{H}_0), \quad k_2 = f_\theta\left(\mathbf{H}_0 + \frac{\tau}{2} k_1\right), \quad \mathbf{U}_r = \mathbf{H}_0 + \tau k_2. \end{aligned} \quad (9)$$

where k_1, k_2 denote intermediate slopes in the RK2 update. The resulting proposals are adaptively fused with attention weights α_p – generated by a Dense→softmax layer – that emphasize the more informative update, while a skip connection preserves the original features \mathbf{H}_0 , thereby producing refined representations \mathbf{U}_{fu} that jointly capture coarse- and fine-grained details as:

$$\mathbf{U}_{fu} = \alpha_p(\mathbf{U}_e + \mathbf{U}_r) + (1 - \alpha_p) \mathbf{H}_0. \quad (10)$$

We achieve Heterogeneous Channel Attention (HCA) (Figure 4 (B)) by applying diverse global pooling oper-

ations – GAP, GMP, GMN, and GSP – to the resulting details (\mathbf{U}_{fu}) to capture diverse channel statistics. We then aggregate the resulting contexts and feed them via a MLP followed by sigmoid, generating a hybrid space attention map (A_{HS}), which is used to reweight channels according to its learned importance to learn enhanced features:

$$A_{\text{HS}} = \sigma(f_{\theta}(\text{GAP}(\mathbf{U}_{\text{fu}}) + \text{GMP}(\mathbf{U}_{\text{fu}}) + \text{GMN}(\mathbf{U}_{\text{fu}}) + \text{GSP}(\mathbf{U}_{\text{fu}}))) \quad (11)$$

$$\mathbf{U}_{\text{out}} = \mathbf{U}_{\text{fu}} \odot A_{\text{HS}}. \quad (12)$$

The output \mathbf{U}_{out} undergoes cyclic shift reversal and window reconstruction to original spatial positions, yielding $\tilde{x}_{i,ws}$ for each window scale ws (Figure 3 (B)). In parallel, the same global pooling operations are applied to frequency-domain tokens \mathbf{F}_t across all windows, followed by fusing them to learn diverse channel descriptors (\mathbf{C}_e) (Figure 3 (A)):

$$\mathbf{C}_e = \text{GAP}(\mathbf{F}_t) + \text{GMP}(\mathbf{F}_t) + \text{GMN}(\mathbf{F}_t) + \text{GSP}(\mathbf{F}_t). \quad (13)$$

We compute the instance-specific attention weights i.e., $\omega_{\text{ins}}^{(i)}$ and ω_g on \mathbf{C}_e and α_p , respectively, and then assign them to $\tilde{x}_{i,ws}$ and leverage SP layer with original input x'_i , resulting the refined representations:

$$\omega_{\text{ins}}^{(i)} = \text{softmax}(\mathbf{C}_e), \quad \omega_g = \alpha_p. \quad (14)$$

$$x'_i = x'_i + \text{SP} \left(\sum_{ws=1}^2 (\omega_{\text{ins},ws}^{(i)} \omega_g, ws) \tilde{x}_{i,ws} \right) \quad (15)$$

(B) Multi-scale Multi-frequency Mutual Update Attention An (MMMUA) block (Figure 5 (A)) jointly learn multimodal information from inputs X' (via Hy-SFA) through mutual cross-modal interactions. Operating at multiple spatial scales and frequency bands, MMMUA generates multi-modal spatial-frequency attention maps A_{D_i} that recalibrate each modality features, learning robust shared representations X^s as:

$$X^s = X' \odot A_{D_i} \odot \omega_i. \quad (16)$$

where channel-wise learnable parameters ω_i for each modality i . To learn multi-modal spatial-frequency attention maps A_{D_i} , the MMMUA module comprises three core components:

- *Frequency-domain channel Information Fusion (FCIF)* component (Figure 5(C)) captures diverse channel dependencies by decomposing modality-specific input (e.g., x'_1) into wavelet sub-bands via wavelet DWC denoted as WDWC: low-low (LL), high-low (HL), low-high (LH), and high-high (HH)². To learn diverse channel cues from each sub-band, we design a Hierarchical Channel Fusion (HCF) scheme (ref. Fig. 1 in the Supplementary) that applies diverse global pooling operations – GAP, GMP, GMN, and GSP – to capture distinct channel contexts i.e., C_{GAP} , C_{GMP} , C_{GMN} , and C_{GSP} . These contexts are fused

²These sub-bands capture coarse-grained structures, horizontal edges, vertical edges, and fine-grained textures, respectively.

via inter-sub-band fusion (Eqs.18–20), integrating parallel and cascaded addition-with-subtraction to learn comprehensive and complementary frequency-domain channel details C_f :

$$\begin{aligned} (\text{LL}, \text{HL}, \text{LH}, \text{HH}) &= \text{WDWC}(x'_1), \\ [C_{\text{Sum}}, C_{\text{Diff}}] &= \text{HCF}(\text{LL}, \text{HL}, \text{LH}, \text{HH}), \\ C_f &= \sum_j \omega_j \odot \text{DR}_j(\text{BN}_j(C_j)) \end{aligned} \quad (17)$$

where $C_j = [C_{\text{Sum}}, C_{\text{Diff}}]$ and DR and BN denote dropout and batch norm. HCF can be written as:

$$\begin{aligned} C_{\text{GAP}} &= \sum_T \text{GAP}(T), \quad C_{\text{GMP}} = \sum_T \text{GMP}(T), \\ C_{\text{GMN}} &= \sum_T \text{GMN}(T), \quad C_{\text{GSP}} = \sum_T \text{GSP}(T) \end{aligned} \quad (18)$$

where $T \in \{\text{LL}, \text{LH}, \text{HL}, \text{HH}\}$.

$$\begin{aligned} C_{\text{Sum}} &= C_{\text{GAP}} + C_{\text{GMP}} + C_{\text{GMN}} + C_{\text{GSP}}, \\ C_{\text{Diff}} &= C_{\text{GMP}} - (C_{\text{GAP}} + C_{\text{GMN}}) \end{aligned} \quad (19)$$

- *Spatial-domain Multi-scale Information Fusion (SMIF)* (Figure 5 (D)) captures fine-grained multi-scale spatial-channel. Specifically, it stacks an MSHC block followed by our SCPFA block from the SCALA module to refine representations (\hat{x}'_m) across scales. Next, diverse global pooling operations – GAP, GMP, GMN, and GSP – are applied to capture complementary channel contexts, which are fused to learn diverse spatial-channel dependencies i.e., C_{SP} as:

$$\begin{aligned} \hat{x}'_m &= \text{SCPFA}(\text{MSHC}(x'_m)), \\ C_{\text{SP}} &= \text{GMP}(\hat{x}'_m) + \text{GAP}(\hat{x}'_m) + \text{GMN}(\hat{x}'_m) + \text{GSP}(\hat{x}'_m). \end{aligned} \quad (20)$$

- *Mutual Cross Bidirectional Interactions (MCBI)* component (Figure 5(B)) is designed to integrate frequency domain channel contexts – i.e., C_f from FCIF with spatial domain spatial-channel details – i.e., C_{SP} from SMIF for multi-modal input X' , facilitating *mutual enhancement through complementary information exchange*. It applies *bidirectional cross-interactions* to fuse C_f of modality x'_1 with C_{SP} of modality x'_m , and vice versa. This asymmetric interaction mutually updates channel dependencies while preserving modality-specific features, capturing complementary cross-domain spatial-channel information. An adaptive scaling factor w_i modulates these interactions to enhance discriminative capacity. Finally, sigmoid activations generate cross-domain attention maps: $A_{D_i} = \text{MMMUA}(\cdot)$, which highlight discriminative regions and jointly optimize spatial-channel coherence across modalities. The attention map is computed as:

$$\begin{aligned} \hat{C}_{\text{SP}} &= \omega_1 \odot C_{\text{SP}} + \omega_2 \odot C_f, \\ \hat{C}_f &= (\text{DR}(\text{BN}(\hat{C}_{\text{SP}})) \odot \omega_3) + (C_f \odot \omega_2), \\ A_{D_i} &= [\sigma_1(\hat{C}_f), \sigma_2(\hat{C}_{\text{SP}})]. \end{aligned} \quad (21)$$

Summary. HyPCA couples parallel spatial–channel fusion in RALA (SCPFA = CHIA || SHIA) with cascaded hybrid-

Table 2. Performance comparison of HyPCA-Net with SOTA methods (M1–M8) on 8 datasets (D1–D8) for classification. Bold/underlined values indicate the best/second-best results, respectively. We report no. of parameters (in millions) and GFLOPS for each method.

Datasets → Models ↓	Backbone	D1: Nickparvar			D2: IQ-OTHNCCD			D3: Tuberculosis			D4: CNMC-2019			D5: HAM10000			D6: SIPaKMeD			D7: CRC			D8: CBIS-DDSM			Overall	
		ACC	F1	AUC	ACC	F1	AUC	ACC	F1	AUC	ACC	F1	AUC	ACC	F1	AUC	ACC	F1	AUC	ACC	F1	AUC	ACC	F1	AUC	#P	#F
DDA-Net	ResNet18	96.8	96.6	97.2	98.1	97.5	98.2	95.8	95.1	95.4	92.2	91.8	92.1	92.2	92.0	92.6	92.5	92.8	91.9	92.7	92.7	93.1	92.5	91.8	91.5	12.1	1.12
MSCAM	PVT-B2	97.6	97.6	97.9	99.5	99.5	99.5	97.8	96.9	97.6	95.3	95.1	95.3	97.6	97.2	97.6	94.2	94.0	94.9	96.4	96.2	96.6	94.1	93.9	94.2	26.9	<u>1.3</u>
MFMSA	ResNet50	97.9	97.7	98.0	99.5	99.3	99.5	98.1	97.3	98.3	95.6	95.2	95.9	97.9	97.4	97.9	94.8	94.4	95.3	96.7	96.5	96.6	94.6	94.5	94.6	26.9	1.4
Gloria	ResNet50	98.1	97.6	97.9	98.5	98.4	98.5	96.6	96.0	96.9	93.3	93.3	93.4	93.8	93.8	94.5	94.2	94.2	94.2	95.9	95.6	95.7	92.5	91.2	91.9	30.8	1.54
MTTU-Net	ResNet50	97.9	97.9	98.0	99.5	99.2	99.5	97.3	96.6	97.6	94.3	93.9	94.1	97.4	96.5	97.2	91.9	92.3	92.6	96.9	96.8	97.0	94.1	93.3	94.5	38.1	6.8
MuMu	ResNet50	96.8	96.8	97.2	98.2	97.9	98.7	97.1	96.4	96.8	93.4	93.1	93.9	92.8	92.4	93.2	92.3	91.7	92.9	95.9	95.3	95.9	92.1	91.6	92.5	56.6	2.97
M ³ Att	Swin-B	97.5	97.4	97.9	98.8	98.7	98.8	96.9	95.6	96.8	94.0	93.6	94.2	95.5	94.9	95.3	92.2	91.5	92.3	96.1	96.2	96.4	93.2	92.7	93.6	183	12.14
DRIFA-Net	ResNet18	98.4	98.4	98.7	99.7	99.5	99.5	98.2	97.5	98.6	96.4	96.3	96.7	98.2	97.9	98.5	95.6	95.5	95.9	97.0	96.8	97.1	95.2	95.1	95.4	53.8	4.83
HyPCA-Net18	ResNet18	98.8	98.7	99.0	99.8	99.8	99.8	98.9	98.0	99.2	97.2	97.1	97.5	99.4	99.3	99.7	95.7	95.7	96.1	98.3	97.9	98.5	96.3	96.2	96.5	14.47	2.25
HyPCA-Net50	ResNet50	99.2	99.1	99.3	99.9	99.9	99.9	99.1	98.3	99.4	97.5	97.3	97.9	99.6	99.6	99.8	96.7	96.4	97.2	98.5	98.1	98.7	96.9	96.6	97.2	28.4	3.03
HyPCA-Net-IN	Inception-v3	98.5	98.4	98.6	99.8	99.8	99.8	98.4	97.7	98.9	96.9	96.9	97.2	100	100	100	97.2	97.2	97.5	98.7	98.7	98.7	97.1	97.1	97.3	26.8	2.76
HyPCA-Net-ViT	ViT-Ti	99.4	99.4	99.3	99.9	99.9	99.9	99.2	98.8	99.2	97.9	97.7	98.1	100	100	100	97.7	97.7	97.7	98.8	98.7	98.8	97.8	97.5	98.2	22.5	3.42

Table 3. Performance comparison of HyPCA-Net-Seg (SegNet backbone) and HyPCA-Net-EMCAD (EMCAD backbone) with SOTA methods on D9–D10 datasets

Model	D9: COVID-19		D10: ISIC		#P	#F
	DSC	IoU	DSC	IoU		
UNet	47.7	38.6	87.3	80.2	34.5	65.5
PolyPVT	81.7	74.4	90.4	83.9	25.1	5.3
MTTU-Net	82.2	75.7	89.2	82.6	71.6	20.9
MADGNet	83.9	76.9	90.2	83.8	31	14.2
PVT-CASCADE	84.1	77.3	90.4	84.0	34.1	7.6
EMCAD	85.8	78.6	90.9	84.1	26.8	<u>5.6</u>
DRIFA-Net	84.4	77.1	90.6	83.9	67.3	19.9
HyPCA-Net-Seg	88.2	80.9	92.7	85.3	21.7	8.04
HyPCA-Net-EMCAD	90.3	82.5	93.8	86.4	18.6	7.65

space, dual-domain modeling in DVCA (Hy-SFA = TFSI → FDCA; MMMUA = FCIF + SMIF + MCBI). The parallel step curbs early information loss, while the cascade fuses token- and frequency-space evidence and synchronizes spatial and frequency cues across modalities (ref. Figs. 2–5). Such parallel → cascaded coupling is new to multimodal fusion in medical imaging and yields higher performance gains at low computational cost (Tables 2–6).

4. Experimental Analysis and Results

Datasets We evaluated HyPCA-Net on ten public medical-imaging benchmarks: For classification we used Nickparvar [26], IQ-OTH NCCD [1], Tuberculosis [32], CNMC-2019 [24], HAM10000 [38], SIPaKMeD [28], CRC [20], CBIS-DDSM [34], denoted as (D1–D8). For segmentation we used COVID-19 lung CT [19] and ISIC2018 skin lesions [6] datasets, denoted as (D9–D10). Images were resized to 128 × 128 × 3 (classification) or 224 × 224 × 3 (segmentation) and a split of 80/10/10 (train/val/test) with standard on-the-fly augmentations was used.

Models We evaluated HyPCA-Net against a comprehensive set of state-of-the-art (SOTA) baselines. For classification, unimodal baselines are DDA-Net, MADGNet’s MFMSA [25], and EMCAD’s MSCAM [31] – denoted as M1–M3; while multimodal fusion baselines comprises Gloria [15], MTTU-Net [5], MuMu [17], M³Att, and DRIFA-Net – denoted as M4–M8. For segmentation, we compare MTTU-Net and DRIFA-Net

(with SegNet decoder), alongside SOTA unimodal baselines: UNet [33], PolypPVT [11], MADGNet, EMCAD, and PVT-CASCADE [30], denoted as M9–M15. Notably, we instantiate HyPCA-Net with four classification backbones – ResNet-18 [13], ResNet-50 [13], Inception-v3 [37], and ViT-Ti [36], and SegNet [2] and EMCAD [31] decoders (paired with our HyPCA-Net18 encoder) for segmentation. These variants are denoted as HyPCA-Net18, HyPCA-Net50, HyPCA-Net-IN, HyPCA-Net-ViT, HyPCA-Net-Seg, and HyPCA-Net-EMCAD.

Notation We report Accuracy (Acc), F1 score (F1), AUC, Dice Score (DSC), Intersection-over-Union (IoU), number of parameters in millions (#P), and GFLOPs (#F) as metrics.

See *supplementary* for dataset, model, and training details.

4.1. Performance Comparisons

We present results in Tables 2 and 3, from which it can be seen that HyPCA-Net achieves exceptional performance on classification and segmentation datasets, with performance ranging from 80.9% to 100%. Compared to SOTA unimodal and multimodal fusion baselines, HyPCA-Net achieves performance improvements of 0.1%–43.9%, while reducing parameters by up to 92% and FLOPs by up to 81.47%. We conducted a qualitative analysis on D1 and D5 datasets as shown in Figure 6, which further validate its effectiveness. See *supplementary* for more details and results.

As we discussed earlier, to address **Challenge 1**, our HyPCA-Net achieves an effective balance between optimal performance and minimal computational cost by incorporating two efficient and effective modules – RALA and DVCA. Because cascaded designs are inherently *sequential*, they process different aspects in isolation, lack joint optimization, and are therefore *limited in preserving holistic information*, ultimately *constraining the richness of learned representations* [23, 35]. In contrast, our hybrid attention design seamlessly integrates parallel fusion attention with cascaded attention to preserve holistic cues while *jointly* and *cascadingly* modeling spatial–channel dependencies in both hybrid space and dual-domain representation learning.

Table 4. Ablation of HyPCA-Net18 modules (left) and components (right), highlighting their contributions to performance gains on D5–D6 datasets.

Integrated modules			D5: HAM10000		D6: SIPaKMeD		Integrated components within module									D5: HAM10000		D6: SIPaKMeD		#P #F	
RALA	Hy-SFA	MMMUUA	F1	F1	#P	MSHC	CHIA	SHIA	FCIF	SMIF	MCBI	TFSI	FDCA	Acc	F1	Acc	F1	#P	#F		
×	×	×	93.2	89.3	23.4	×	×	×	×	×	×	×	×	93.2	93.1	89.5	89.3	23.4	1.16		
×	×	✓	97.1	93.0	25.2	✓	✓	×	✓	×	×	✓	×	96.8	96.6	92.9	92.8	11.1	1.8		
×	✓	✗	96.7	92.8	28.1	✓	✓	✗	✓	✗	×	✓	✗	97.6	97.6	93.9	93.7	12.4	1.9		
×	✓	✓	<u>98.6</u>	<u>94.9</u>	30.5	✗	✗	✓	✓	✗	×	✓	✗	97.3	97.2	93.6	93.4	28.6	2.84		
✓	✗	✗	96.1	92.3	10.1	✓	✓	✓	✓	✗	×	✓	✗	97.9	97.7	94.3	94.2	12.7	1.92		
✓	✗	✓	97.8	93.8	<u>11.9</u>	✓	✗	✗	✓	✓	✓	✓	✗	98.3	98.3	94.3	94.0	<u>11.7</u>	1.85		
✓	✓	✗	97.3	93.4	12.9	✓	✓	✓	✓	✓	✓	✓	✗	<u>98.7</u>	<u>98.7</u>	<u>95.3</u>	<u>95.1</u>	13.4	1.91		
✓	✓	✓	99.3	95.7	14.5	✓	✓	✓	✓	✓	✓	✓	✓	99.4	99.3	95.7	95.7	14.5	2.25		

Table 5. Ablation of HyPCA-Net–EMCAD modules (left) and components (right), highlighting their contributions to performance gains on D9–D10 datasets.

Integrated modules			D9: COVID-19		D10: ISIC		Integrated components within module									D9: COVID-19		D10: ISIC		#P #F	
RALA	Hy-SFA	MMMUUA	DSC	IoU	DSC	IoU	#P	MSHC	CHIA	SHIA	FCIF	SMIF	MCBI	TFSI	FDCA	DSC	IoU	DSC	IoU	#P	#F
×	×	✗	82.8	75.5	85.9	79.1	27.2	✗	✗	✗	✗	✗	✗	✗	✗	82.8	75.5	85.9	79.1	27.2	4.32
×	✗	✓	86.2	78.8	89.1	81.9	29.2	✓	✗	✗	✓	✗	✗	✓	✗	85.5	78.2	87.4	81.2	15.1	6.27
×	✓	✗	85.5	77.9	88.4	81.1	32.1	✓	✓	✗	✓	✗	✗	✓	✗	86.5	79.1	88.9	82.5	16.2	6.58
×	✓	✓	<u>88.5</u>	<u>80.9</u>	<u>90.7</u>	<u>84.1</u>	34.4	✗	✗	✓	✓	✗	✗	✓	✗	86.2	78.8	88.5	82.1	32.4	9.46
✓	✗	✗	84.7	77.4	87.9	80.8	13.9	✓	✓	✓	✓	✗	✗	✓	✗	86.8	79.5	89.3	82.8	16.5	6.64
✓	✗	✓	88.1	80.6	91.2	83.6	<u>15.7</u>	✓	✗	✗	✓	✓	✓	✓	✗	87.6	80.1	90.6	83.7	<u>15.5</u>	6.43
✓	✓	✗	87.4	79.7	90.3	82.8	16.6	✓	✓	✓	✓	✓	✓	✓	✗	<u>89.1</u>	<u>81.0</u>	<u>92.7</u>	<u>85.5</u>	17.2	6.61
✓	✓	✓	90.3	82.5	93.8	86.4	18.6	✓	✓	✓	✓	✓	✓	✓	✓	90.3	82.5	93.8	86.4	18.6	7.65

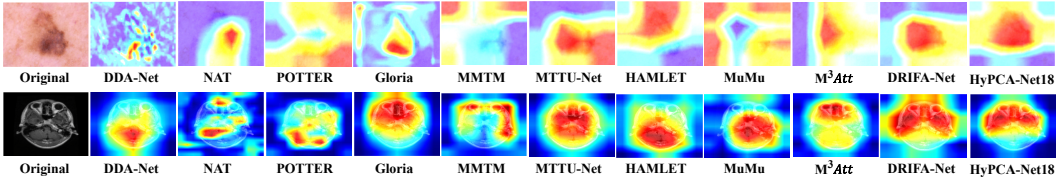


Figure 6. Visual representation of the important regions highlighted by our proposed HyPCA-Net framework and ten other SOTA methods using the GRAD-CAM technique on two benchmark datasets D5 and D1.

Table 6. Performance comparison (F1-score) of cascaded (CA) vs. hybrid (HA) attention in CHIA and SHIA on D5 and D6, keeping other components fixed.

HA	CA	D5	D6	#P	#F
✓	✗	99.3	95.7	14.47	2.25
✗	✓	98.9	95.2	14.47	2.25

As a result, HyPCA-Net overcomes the intrinsic drawbacks of purely cascaded schemes and directly addresses **Challenge 2**, yielding more robust shared representation learning. *See discussion part of [supplementary](#) material.*

4.2. Ablation Study

We evaluated key components of HyPCA-Net on datasets D5–D6 and D9–D10, focusing on the RALA (with SCPFA), and Hy-SFA and MMMUA modules within DVCA. Tables 4–5 show that HyPCA-Net outperforms its ablated variants by 0.4% – 7.9%, highlighting the effectiveness of its hybrid attention design. Further, we analyzed contributions from individual modules: MSHA, CHIA, and SHIA in SCALA; FCIF, SMIF, and MCBI in MMMUA; and TFSI and FDCA in Hy-SFA (Tables 4–5). HyPCA-Net achieves up to 7.9% performance improvements over partial configurations, emphasizing the complementary roles of these modules. Finally, we compare cascaded (CHIA → SHIA → DVCA) and hybrid (parallel CHIA + SHIA → DVCA) configurations (Table 6); The hybrid variant achieves a 0.4% – 0.5% performance gain, capturing more robust shared representations at lower computational cost.

One can infer that the limited performance of the ablated variants (Tables 4–5) arises from their inability to learn robust shared representations at low computational cost—essential for **addressing challenge 1**. To **address challenge 2**, we note that cascaded attention architectures face progressive information loss due to the absence of *parallel-cascaded (hybrid) fusion*, which hinders holistic information preservation and weakens representation learning, ultimately lowering performance (Table 6) [23, 35]. As discussed earlier, HyPCA-Net addresses both challenges through its integrated hybrid attention modules (RALA, Hy-SFA, and MMMUA). Specifically, RALA efficiently captures multi-scale spatial–channel dependencies via parallel fusion, while Hy-SFA and MMMUA model complementary dual-domain interactions. Our hybrid framework preserves holistic information, improving multi-disease classification with low cost (see [supplementary](#) for more results)

5. Conclusion

We present HyPCA-Net, an efficient multimodal fusion framework designed for advancing medical image analysis, making it highly suitable for real-world medical AI applications. HyPCA-Net is evaluated on ten diverse datasets, demonstrating strong generalizability across medical imaging modalities. It outperforms leading baselines with up to ≈ 5.2% higher performance and ≈ 73.1% lower computational cost. In the future, we are interested in integrating *adversarial robustness*, and *domain-shift adaptation* into

References

- [1] Hamdalla Alyasriy and A Muayed. The iq-othncd lung cancer dataset. *Mendeley Data*, 1(1):1–13, 2020. [7](#)
- [2] Vijay Badrinarayanan, Alex Kendall, and Roberto Cipolla. Segnet: A deep convolutional encoder-decoder architecture for image segmentation. *IEEE transactions on pattern analysis and machine intelligence*, 39(12):2481–2495, 2017. [7](#)
- [3] Debasish Das Chakladar, Pradeep Kumar, Partha Pratim Roy, Debi Prosad Dogra, Erik Scheme, and Victor Chang. A multimodal-siamese neural network (msnn) for person verification using signatures and EEG. *Information Fusion*, 71: 17–27, 2021. [2](#)
- [4] Ricky T. Q. Chen, Yulia Rubanova, Jesse Bettencourt, and David K. Duvenaud. Neural ordinary differential equations. In *Advances in Neural Information Processing Systems (NeurIPS)*, 2018. [5](#)
- [5] J. Cheng, J. Liu, H. Kuang, and J. Wang. A fully automated multimodal mri-based multi-task learning for glioma segmentation and idh genotyping. *IEEE Transactions on Medical Imaging*, 41(6):1520–1532, 2022. [2, 7](#)
- [6] Noel Codella, Veronica Rotemberg, Philipp Tschandl, M Emre Celebi, Stephen Dusza, David Gutman, Brian Helba, Aadi Kalloo, Konstantinos Liopyris, Michael Marchetti, et al. Skin lesion analysis toward melanoma detection 2018: A challenge hosted by the international skin imaging collaboration (isic). *arXiv preprint arXiv:1902.03368*, 2019. [7](#)
- [7] Y. Cui, Y. Tao, W. Ren, and A. Knoll. Dual-domain attention for image deblurring. In *Proceedings of the AAAI Conference on Artificial Intelligence*, pages 479–487, 2023. [1, 2](#)
- [8] Khakon Das, Ashish Khare, Debasish Das Chakladar, and Dinesh Jaluka. Fusion in medical imaging techniques for enhancing stroke region detection: A selective review. In *International Conference on Pattern Recognition*, pages 167–179. Springer, 2024. [2](#)
- [9] Joy Dhar, Kapil Rana, and Puneet Goyal. Uncertainty-rifanet: Uncertainty aware robust information fusion attention network for brain tumors classification in mri images. In *International Conference on Pattern Recognition*, pages 311–327. Springer, 2024. [1](#)
- [10] Joy Dhar, Nayyar Zaidi, Maryam Haghigiat, Sudipta Roy, Puneet Goyal, Azadeh Alavi, and Vikas Kumar. Multimodal fusion learning with dual attention for medical imaging. In *2025 IEEE/CVF Winter Conference on Applications of Computer Vision (WACV)*, pages 4362–4371. IEEE, 2025. [1, 2, 3](#)
- [11] Bo Dong, Wenhui Wang, Deng-Ping Fan, Jinpeng Li, Huazhu Fu, and Ling Shao. Polyp-pvt: Polyp segmentation with pyramid vision transformers. *arXiv preprint arXiv:2108.06932*, 2021. [7](#)
- [12] Ali Hassani, Steven Walton, Jiachen Li, Shen Li, and Humphrey Shi. Neighborhood attention transformer. In *Proceedings of the IEEE/CVF Conference on Computer Vision and Pattern Recognition*, pages 6185–6194, 2023. [1, 2](#)
- [13] Kaiming He, Xiangyu Zhang, Shaoqing Ren, and Jian Sun. Deep residual learning for image recognition. In *Proceedings of the IEEE conference on computer vision and pattern recognition*, pages 770–778, 2016. [7](#)
- [14] X. He, Y. Wang, S. Zhao, and X. Chen. Co-attention fusion network for multimodal skin cancer diagnosis. *Pattern Recognition*, 133:108990, 2023. [2, 3](#)
- [15] S. C. Huang, L. Shen, M. P. Lungren, and S. Yeung. Gloria: A multimodal global-local representation learning framework for label-efficient medical image recognition. In *Proceedings of the IEEE/CVF International Conference on Computer Vision*, pages 3942–3951, 2021. [2, 3, 7](#)
- [16] Md Mofijul Islam and Tariq Iqbal. Hamlet: A hierarchical multimodal attention-based human activity recognition algorithm. In *2020 IEEE/RSJ International Conference on Intelligent Robots and Systems (IROS)*, pages 10285–10292. IEEE, 2020. [1, 2, 3](#)
- [17] M. M. Islam and T. Iqbal. Mumu: Cooperative multitask learning-based guided multimodal fusion. In *Proceedings of the AAAI Conference on Artificial Intelligence*, pages 1043–1051, 2022. [1, 2, 3, 7](#)
- [18] Hamid Reza Vaezi Jozé, Amirreza Shaban, Michael L Iuzolino, and Kazuhito Koishida. Mmtm: Multimodal transfer module for cnn fusion. In *Proceedings of the IEEE/CVF conference on computer vision and pattern recognition*, pages 13289–13299, 2020. [2](#)
- [19] Ma Jun, Ge Cheng, Wang Yixin, An Xingle, Gao Jiantao, Yu Ziqi, Zhang Minqing, Liu Xin, Deng Xueyuan, Cao Shucheng, et al. Covid-19 ct lung and infection segmentation dataset. (*No Title*), 2020. [7](#)
- [20] Jakob Nikolas Kather, Cleo-Aron Weis, Francesco Bianconi, Susanne M Melchers, Lothar R Schad, Timo Gaiser, Alexander Marx, and Frank Gerrit Zöllner. Multi-class texture analysis in colorectal cancer histology. *Scientific reports*, 6(1): 1–11, 2016. [7](#)
- [21] Chang Liu, Henghui Ding, Yulun Zhang, and Xudong Jiang. Multi-modal mutual attention and iterative interaction for referring image segmentation. *IEEE Transactions on Image Processing*, 32:3054–3065, 2023. [2, 3](#)
- [22] Ze Liu, Yutong Lin, Yue Cao, Han Hu, Yixuan Wei, Zheng Zhang, Stephen Lin, and Baining Guo. Swin transformer: Hierarchical vision transformer using shifted windows. In *Proceedings of the IEEE/CVF International Conference on Computer Vision (ICCV)*, pages 10012–10022, 2021. [5](#)
- [23] Cheng Lv, Enxu Zhang, Guowei Qi, Fei Li, and Jiaofei Huo. A lightweight parallel attention residual network for tile defect recognition. *Scientific Reports*, 14(1):21872, 2024. [2, 7, 8](#)
- [24] S Mourya, S Kant, P Kumar, A Gupta, and R Gupta. All challenge dataset of isbi 2019. *The Cancer Imaging Archive*, 2019. [7](#)
- [25] Ju-Hyeon Nam, Nur Suriza Syazwany, Su Jung Kim, and Sang-Chul Lee. Modality-agnostic domain generalizable medical image segmentation by multi-frequency in multi-scale attention. In *Proceedings of the IEEE/CVF Conference on Computer Vision and Pattern Recognition*, pages 11480–11491, 2024. [2, 7](#)

[26] Msoud Nickparvar. Brain tumor MRI dataset. Data set, 2021. Accessed on 3rd March. [7](#)

[27] Xiaokang Peng, Yake Wei, Andong Deng, Dong Wang, and Di Hu. Balanced multimodal learning via on-the-fly gradient modulation. In *Proceedings of the IEEE/CVF conference on computer vision and pattern recognition*, pages 8238–8247, 2022. [2](#)

[28] Maria E Plissiti, Panagiotis Dimitrakopoulos, Giorgos Sifakis, Christophoros Nikou, Orestis Krikoni, and Avraam Charchanti. Sipakmed: A new dataset for feature and image based classification of normal and pathological cervical cells in pap smear images. In *2018 25th IEEE International Conference on Image Processing (ICIP)*, pages 3144–3148. IEEE, 2018. [7](#)

[29] Zequn Qin, Pengyi Zhang, Fei Wu, and Xi Li. Fcanet: Frequency channel attention networks. In *Proceedings of the IEEE/CVF International Conference on Computer Vision (ICCV)*, pages 783–792, 2021. [5](#)

[30] Md Mostafijur Rahman and Radu Marculescu. Medical image segmentation via cascaded attention decoding. In *Proceedings of the IEEE/CVF winter conference on applications of computer vision*, pages 6222–6231, 2023. [7](#)

[31] Md Mostafijur Rahman, Mustafa Munir, and Radu Marculescu. Emcad: Efficient multi-scale convolutional attention decoding for medical image segmentation. In *Proceedings of the IEEE/CVF Conference on Computer Vision and Pattern Recognition*, pages 11769–11779, 2024. [4, 7](#)

[32] Tawsifur Rahman, Amith Khandakar, Muhammad Abdul Kadir, Khandaker Rejaul Islam, Khandakar F Islam, Rashid Mazhar, Tahir Hamid, Mohammad Tariqul Islam, Saad Kashem, Zaid Bin Mahbub, et al. Reliable tuberculosis detection using chest x-ray with deep learning, segmentation and visualization. *Ieee Access*, 8:191586–191601, 2020. [7](#)

[33] Olaf Ronneberger, Philipp Fischer, and Thomas Brox. U-net: Convolutional networks for biomedical image segmentation. In *Medical image computing and computer-assisted intervention–MICCAI 2015: 18th international conference, Munich, Germany, October 5-9, 2015, proceedings, part III 18*, pages 234–241. Springer, 2015. [7](#)

[34] R Sawyer-Lee, F Gimenez, A Hoogi, and D Rubin. Curated breast imaging subset of digital database for screening mammography (cbis-ddsm)[skup podataka]. *The cancer imaging archive*, 2016. [7](#)

[35] Yunhang Shen, Liujuan Cao, Zhiwei Chen, Baochang Zhang, Chi Su, Yongjian Wu, Feiyue Huang, and Rongrong Ji. Parallel detection-and-segmentation learning for weakly supervised instance segmentation. In *Proceedings of the IEEE/CVF International Conference on Computer Vision*, pages 8198–8208, 2021. [2, 7, 8](#)

[36] Andreas Steiner, Alexander Kolesnikov, Xiaohua Zhai, Ross Wightman, Jakob Uszkoreit, and Lucas Beyer. How to train your vit? data, augmentation, and regularization in vision transformers. *arXiv preprint arXiv:2106.10270*, 2021. [7](#)

[37] Christian Szegedy, Vincent Vanhoucke, Sergey Ioffe, Jon Shlens, and Zbigniew Wojna. Rethinking the inception architecture for computer vision. In *Proceedings of the IEEE conference on computer vision and pattern recognition*, pages 2818–2826, 2016. [7](#)

[38] Philipp Tschandl, Cliff Rosendahl, and Harald Kittler. The ham10000 dataset, a large collection of multi-source dermatoscopic images of common pigmented skin lesions. *Scientific data*, 5(1):1–9, 2018. [7](#)

[39] Ce Zheng, Xianpeng Liu, Guo-Jun Qi, and Chen Chen. Potter: Pooling attention transformer for efficient human mesh recovery. In *Proceedings of the IEEE/CVF Conference on Computer Vision and Pattern Recognition*, pages 1611–1620, 2023. [1, 2](#)